

Analytical Green's Function of Multidimensional Boltzmann Transport Equation for Modeling Hydrodynamic Second Sound

Xin Qian^{1*}, Chuang Zhang², Te-Huan Liu^{1*}, and Ronggui Yang^{1,3*}

¹ School of Energy and Power Engineering, Huazhong University of Science and Technology, Wuhan 430074, China.

² Department of Physics, Hangzhou Dianzi University, Hangzhou 310018, China.

³ College of Engineering, Peking University, Beijing 100871, China.

Corresponding Emails: xinqian21@hust.edu.cn, thliu@hust.edu.cn, ronggui@pku.edu.cn

ABSTRACT

Hydrodynamic second sound can be generated by heat pulses when the phonon-phonon interaction is dominantly momentum conserving, and the propagation of the temperature field becomes wavelike rather than diffusive. While the Boltzmann transport equation (BTE) has been widely applied to study phonon dynamics and thermal transport at the nanoscale, modeling the hydrodynamic transport regime remains challenging. The widely used relaxation time approximation (RTA) treats all phonon interactions as resistive without considering momentum conservation, resulting in the absence of phonon hydrodynamics. Rigorously solving BTE by inverting the full scattering matrix, however, is extremely computationally demanding and has been only applied to model one-dimensional temperature variations. Here, we present an analytical Green's function formalism for solving multidimensional Boltzmann transport equation (BTE) using phonon properties from first-principles calculations. This formalism involves Callaway's scattering approximation with separate relaxation times for momentum-conserving and momentum-destroying scattering events. The Green's function captures phonon dynamics in a wide range of temperature, spatial, and temporal scales, and successfully reproduces the transition from ballistic, hydrodynamic, to diffusive transport regimes. Our method avoids the computationally demanding inversion of large scattering matrices and shows good accuracies in predicting the temperature oscillation in ultrafast pump-probe characterizations with different geometries of thermal excitation.

Keywords: second sound; phonon hydrodynamics, Green's function, Boltzmann transport equation.

I. INTRODUCTION

Thermal transport in semiconductors or dielectrics is typically governed by the random walk of phonons¹. Such diffusive transport regime breaks down at small lengths or time scales when phonons transport ballistically without experiencing enough scattering to establish a local equilibrium^{2, 3}. Ballistic transport of phonons has been studied extensively⁴⁻⁹ due to the significance in engineering thermal conductivity of functional materials, and thermal management of nano/microelectronic devices. In contrast to ballistic transport, hydrodynamic phonon transport emerges when phonon-phonon interaction is frequent and mostly momentum-conserving^{10, 11}. In the hydrodynamic regime, the propagation of the temperature field becomes wavelike under pulsed heating, which is known as the second sound¹². The second sound was first observed in superfluid He below 2 K¹³, and later in solids such as Bi at 1.2 K ~ 4 K¹⁴ and NaF in 10 ~ 18 K¹⁵. Such “wavelike” transport of heat energy can serve as an efficient vehicle for removing heat from hot spots, but it was only observed at cryogenic temperatures for nearly 50 years. It was not until the recent few years that research interests in second sound was renewed due to the prediction and observation of second sound in graphitic materials close to room temperature (100 ~ 200 K)¹⁶⁻¹⁸, and the discovery of wavelike signatures in thermal phase lags under rapidly varying temperature field in Ge at room temperature¹⁹.

Theoretically, the second sound can be modeled phenomenologically using a damped wave equation (DWE)^{20, 21}, manybody correlation functions²², or the Boltzmann transport equation (BTE)^{18, 23}. While the DWE provides a convenient way to study the wavy transport behaviors and to process photothermal measurement signals for identifying second sound, it lacks the power to predict the temperatures and lengthscales for realizing wavelike thermal transport, as the coherence time of second sound (τ_{ss}) and the propagation length is treated as empirical parameters to be fitted from experimental data^{20, 21}. On the other hand, the correlation function formulation developed by Enz²² was underpinned by studying the

evolution of local equilibrium density matrices, from which the dispersion relation and frequency window for observing second sound can be derived without empirical parameters. However, direct comparisons between the local correlation function theory with experimental results are usually difficult, due to the experimental challenges in directly probing spatial or temporal correlation functions in temperature or phonon momentum. The theoretical framework of BTE has been widely used for studying phonon transport, including first-principles prediction of thermal conductivity^{24, 25}, modeling temperature and heat dissipation in nanodevices^{9, 26}, and in studying hydrodynamic phonon transport²³. The scattering term in BTE is either treated under relaxation time approximation (RTA) or fully calculated by first-principles anharmonic lattice dynamics. RTA assumes all phonon-phonon scattering events as resistive. It will not only underestimate the thermal conductivity of materials with strong N-scattering such as graphite and diamond, but also miss the entire hydrodynamic phonon transport regime due to the lack of momentum conservation for N-scattering processes. On the other hand, solving BTE with the full scattering matrix can effectively capture the collective phonon dynamics as the momentum conservation is automatically satisfied²⁷. This has been done by iterative solution in thermal conductivity calculations, while most of the phonon transport modeling involving localized hot spots and interfaces has been performed under RTA^{26, 28}. Recently, Chiloyan *et al.*²⁹ derived the exact Green's function of BTE by inverting the full scattering matrix and modeled second-sound mediated temperature oscillations in transient thermal grating (TTG) experiments. Inverting the full scattering matrix is extremely expensive, especially with a dense mesh in the Brillouin zone, such that only one-dimensional problems are computationally feasible. Compared with RTA, Callaway's scattering approximation (CSA) with two distinct relaxation times for N- and R-scattering events represents a better approximation to the full scattering matrix, and it has been widely used in analyzing steady-state hydrodynamic transport, including the Knudsen minimum³⁰ and the

phonon Poiseuille flow¹⁸. While the direct numerical solution of BTE under CSA has been performed for both steady-state and transient phonon transport in various geometries³¹⁻³⁴, gray model or empirical phonon lifetime relations are typically used for phonon dispersions and relaxation times, with few studies on steady-state hydrodynamic transport have incorporated *ab initio* phonon properties in the entire Brillouin zone³⁵.

In this work, we derived the analytical expression for Green's function of multi-dimensional BTE under CSA (hereafter abbreviated as GF-CSA), which can be used to predict transient temperature responses to arbitrary shape of heat sources in infinite or semi-infinite domains, using fully first-principle phonon dispersions and lifetimes. Compared with the GF calculated by inverting the full scattering matrix, the separation of N and R processes in CSA enabled analyzing the asymptotic behavior and phonon dynamics at different scattering limits. We analytically showed that: (i) the damped wave equation emerges from the GF-CSA formalism when N-scattering is dominating, (ii) the GF-CSA reduces asymptotically to RTA when R-scattering is dominating, and (iii) the ballistic and Fourier transport regime is restored at the limits $\Omega\tau \gg 1$ and $\Omega\tau \ll 1$ respectively, with Ω the heating frequency and τ the phonon relaxation time. Finally, GF-CSA successfully captures the temperature oscillations in TTG and transient thermoreflectance with a ring-shaped heat source (ring-TTR), showing excellent agreement with experimental observations. Our work provides a simple formalism for modeling multi-dimensional and transient hydrodynamic phonon transport.

II. THEORETICAL DERIVATION OF GREEN'S FUNCTION

To obtain the Green's function of hydrodynamic phonon transport, we consider solving the BTE under point heat pulse:

$$\frac{\partial n_\mu}{\partial t} + \mathbf{v}_\mu \cdot \nabla n_\mu = \frac{n_\mu^0(T_R) - n_\mu}{\tau_\mu^R} + \frac{n_\mu^d(T_N) - n_\mu}{\tau_\mu^N} + \frac{\dot{Q}_\mu}{\hbar\omega_\mu} \delta(\mathbf{r})\delta(t), \quad (1)$$

where the subscript $\mu = (\mathbf{q}, s)$ denotes the phonon mode with wavevector \mathbf{q} at the s -th phonon branch, n_μ is the nonequilibrium phonon distribution, $v_\mu = \nabla_{\mathbf{q}} \omega_\mu$ is the group velocity (ω_μ is the angular frequency of phonon mode μ), τ_μ^N and τ_μ^R are respectively the relaxation time for momentum-conserving N processes and momentum-reversing R-scattering events, including the Umklapp processes, isotope scattering, and boundary scattering. \dot{Q}_μ is the modal energy generation rate; $\delta(\mathbf{r})$ and $\delta(t)$ are the Dirac functions in the spatial and time domain, respectively. For each mode, the energy generation rate is determined by the mode-specific heat $\dot{Q}_\mu = C_\mu \dot{Q}_0 / \sum_\mu C_\mu$, with \dot{Q}_0 representing the total energy generation rate. n_μ^0 and n_μ^d are correspondingly the local equilibrium and the drifted equilibrium distributions:

$$n_\mu^0(T_R) = \frac{1}{\exp\left(\frac{\hbar\omega_\mu}{k_B T_R(\mathbf{r})}\right) - 1} \quad (2)$$

$$n_\mu^d(T_N, \mathbf{u}) = \frac{1}{\exp\left[\frac{\hbar(\omega_\mu - \mathbf{q} \cdot \mathbf{u})}{k_B T_N(\mathbf{r})}\right] - 1} \quad (3)$$

Here, \mathbf{q} is the phonon wavevector, and \mathbf{u} is a collective drift velocity independent of phonon mode indices. $T_R(\mathbf{r})$ and $T_N(\mathbf{r})$ are pseudo-temperatures for the local equilibrium of R-scattering and N-scattering events³⁴, respectively.

In the near-equilibrium transport regime, deviation in phonon populations can be linearized:

$$n_\mu - n_\mu^0(T_R) = n_\mu^1 - \frac{C_\mu \Delta T_R}{\hbar\omega_\mu}, \quad (4)$$

$$n_\mu - n_\mu^d(T_N) = n_\mu^1 - \left(\frac{C_\mu \Delta T_N}{\hbar\omega_\mu} + \frac{C_\mu T_0}{\hbar\omega_\mu^2} \mathbf{q} \cdot \mathbf{u} \right) \quad (5)$$

where $n_\mu^1 = n_\mu - n_\mu^0(T_0)$ is the deviation in phonon populations from thermal equilibrium at the temperature T_0 . Pseudo-temperature changes are defined as $\Delta T_{N,R} = T_{N,R} - T_0$, and $C_\mu = k_B (\hbar\omega_\mu / k_B T_0)^2 [n_\mu^0 (n_\mu^0 + 1)]$ is the specific heat of mode μ . By defining the energy deviation $g_\mu = \hbar\omega_\mu n_\mu^1$ and by substituting Eqs. (4-5) into Eq. (1), the BTE is simplified to:

$$\frac{\partial g_\mu}{\partial t} + \mathbf{v}_\mu \cdot \nabla g_\mu = \frac{C_\mu \Delta T_R - g_\mu}{\tau_\mu^R} + \frac{C_\mu \Delta T_N - g_\mu}{\tau_\mu^N} + \frac{C_\mu T_0}{\omega_\mu \tau_\mu^N} \mathbf{q} \cdot \mathbf{u} + \dot{Q}_\mu \delta(\mathbf{r}) \delta(t) \quad (6)$$

We now consider solving this equation in a semi-infinite domain with a specular boundary condition at the surface. Under this assumption, the domain can be extended to infinity with even symmetry. While this approach eliminates the consideration of (partially) diffusively boundary and finite thickness effects, but still leaves a wide range of problems that can be solved such as multi-dimensional heat transport in transient thermal grating, and pump-probe thermorefectance experiments. By performing the Fourier transform over the time and space coordinates $(t, \mathbf{r}) \rightarrow (\Omega, \boldsymbol{\xi})$, the energy deviation can be expressed as:

$$g_\mu = \chi_\mu \left[C_\mu (\rho_\mu \Delta T_R + \eta_\mu \Delta T_N) + C_\mu T_0 \eta_\mu \frac{\mathbf{q} \cdot \mathbf{u}}{\omega_\mu} + \dot{Q}_\mu \tau_\mu \right], \quad (7)$$

where $\tau_\mu = 1 / (\tau_\mu^{N-1} + \tau_\mu^{R-1})$ is the total relaxation time, $\rho_\mu = \tau_\mu / \tau_\mu^R$ is the relative strength of R-scattering events, $\eta_\mu = \tau_\mu / \tau_\mu^N$ is the relative strength of N-scattering events, and $\rho_\mu + \eta_\mu \equiv 1$. When $\eta_\mu \rightarrow 0$, the Callaway scattering model decays to simple RTA, and $\eta_\mu \rightarrow 1$ corresponds to the limit of all scatterings being momentum-conserving. The susceptibility χ_μ is defined as:

$$\chi_\mu = \frac{1}{1 + i\Omega \tau_\mu + i\mathbf{F}_\mu \cdot \boldsymbol{\xi}}, \quad (8)$$

where \mathbf{F}_μ denotes the mean free displacement (MFD) and can be obtained by iteratively solving the BTE, as implemented in the ShengBTE package²⁴. Using the MFDs, phonon mean free paths and the relaxation times are calculated as:

$$\Lambda_\mu = \frac{\mathbf{v}_\mu \cdot \mathbf{F}_\mu}{|\mathbf{v}_\mu|}, \quad \tau_\mu = \frac{\mathbf{v}_\mu \cdot \mathbf{F}_\mu}{\mathbf{v}_\mu \cdot \mathbf{v}_\mu} \quad (9)$$

The pseudo-temperatures ΔT_N , ΔT_R , and the collective drive velocity \mathbf{u} in Eq. (7) are the unknowns to be determined. To close the problem, the momentum- and energy-conserving constraints need to be considered. In hydrodynamic phonon transport, both the R- and N-scattering events conserve the thermal energy:

$$\sum_{\mu} \frac{1}{\tau_{\mu}^R} (C_{\mu} \Delta T_R - g_{\mu}) = 0 \quad (10)$$

$$\sum_{\mu} \frac{1}{\tau_{\mu}^N} (C_{\mu} \Delta T_N - g_{\mu}) = 0 \quad (11)$$

Substituting Eq. (7) into Eqs. (10-11), a set of relations correlating ΔT_R , ΔT_N , and the drift velocity \mathbf{u} is established:

$$\left[\sum_{\mu} \frac{C_{\mu}}{\tau_{\mu}^R} (1 - \rho_{\mu} \chi_{\mu}) \right] \Delta T_R - \left(\sum_{\mu} \frac{C_{\mu}}{\tau_{\mu}^R} \eta_{\mu} \chi_{\mu} \right) \Delta T_N - \left(\sum_{\mu} \frac{C_{\mu} T_0 \mathbf{q}}{\omega_{\mu} \tau_{\mu}^N} \rho_{\mu} \chi_{\mu} \right) \cdot \mathbf{u} = \sum_{\mu} \rho_{\mu} \chi_{\mu} \dot{Q}_{\mu} \quad (12)$$

$$\left(- \sum_{\mu} \frac{C_{\mu}}{\tau_{\mu}^N} \rho_{\mu} \chi_{\mu} \right) \Delta T_R + \left[\sum_{\mu} \frac{C_{\mu}}{\tau_{\mu}^N} (1 - \eta_{\mu} \chi_{\mu}) \right] \Delta T_N - \left[\sum_{\mu} \frac{C_{\mu} T_0 \mathbf{q}}{\omega_{\mu} \tau_{\mu}^N} (1 - \eta_{\mu} \chi_{\mu}) \right] \cdot \mathbf{u} = \sum_{\mu} \eta_{\mu} \chi_{\mu} \dot{Q}_{\mu} \quad (13)$$

An additional equation is needed to determine the drift velocity \mathbf{u} . Since N scattering conserves momentum, the following relation holds:

$$\sum_{\mu} \frac{\hbar \mathbf{q}}{\tau_{\mu}^N} [n_{\mu} - n_{\mu}^d(T_N)] = 0 \quad (14)$$

Substituting Eq. (5) and (7) into Eq. (14), we obtained:

$$\begin{aligned} & - \left(\sum_{\mu} \frac{C_{\mu} \mathbf{q}}{\omega_{\mu} \tau_{\mu}^N} \rho_{\mu} \chi_{\mu} \right) \Delta T_R + \left[\sum_{\mu} \frac{C_{\mu} \mathbf{q}}{\omega_{\mu} \tau_{\mu}^N} (1 - \eta_{\mu} \chi_{\mu}) \right] \Delta T_N - \left[\sum_{\mu} \frac{C_{\mu} T_0 \mathbf{q} \mathbf{q}^T}{\omega_{\mu}^2 \tau_{\mu}^N} (1 - \eta_{\mu} \chi_{\mu}) \right] \cdot \mathbf{u} \\ & = \sum_{\mu} \eta_{\mu} \chi_{\mu} \frac{\dot{Q}_{\mu} \mathbf{q}}{\omega_{\mu}} \end{aligned} \quad (15)$$

Eqs. (12), (13), and (15) are all equations necessary to solve the unknown pseudo-temperatures and drift velocities, and they can be rewritten in the linear form:

$$\mathbf{A} \mathbf{X} = \mathbf{b} \quad (16)$$

The linear matrix \mathbf{A} takes the form:

$$\mathbf{A} = \begin{bmatrix} \sum_{\mu} \frac{C_{\mu}}{\tau_{\mu}^R} (1 - \rho_{\mu} \chi_{\mu}) & - \sum_{\mu} C_{\mu} \frac{\tau_{\mu}}{\tau_{\mu}^R \tau_{\mu}^N} \chi_{\mu} & - \sum_{\mu} \frac{C_{\mu} T_0 \mathbf{q}^T}{\omega_{\mu}} \frac{\tau_{\mu}}{\tau_{\mu}^R \tau_{\mu}^N} \chi_{\mu} \\ - \sum_{\mu} C_{\mu} \frac{\tau_{\mu}}{\tau_{\mu}^R \tau_{\mu}^N} \chi_{\mu} & \sum_{\mu} \frac{C_{\mu}}{\tau_{\mu}^N} (1 - \eta_{\mu} \chi_{\mu}) & \sum_{\mu} \frac{C_{\mu} T_0 \mathbf{q}^T}{\omega_{\mu} \tau_{\mu}^N} (1 - \eta_{\mu} \chi_{\mu}) \\ - \sum_{\mu} \frac{C_{\mu} \mathbf{q}}{\omega_{\mu}} \frac{\tau_{\mu}}{\tau_{\mu}^R \tau_{\mu}^N} \chi_{\mu} & \sum_{\mu} \frac{C_{\mu} \mathbf{q}}{\omega_{\mu} \tau_{\mu}^N} (1 - \eta_{\mu} \chi_{\mu}) & \sum_{\mu} \frac{C_{\mu} T_0 \mathbf{q} \mathbf{q}^T}{\omega_{\mu}^2 \tau_{\mu}^N} (1 - \eta_{\mu} \chi_{\mu}) \end{bmatrix}, \quad (17)$$

where the wave vector \mathbf{q} is written in column, and the superscript T denotes the matrix transpose, $\mathbf{q}\mathbf{q}$ is the dyadic product. The vector \mathbf{X} is the thermal responses in pseudo-temperatures and drift velocities to pulsed point heat source, and the vector \mathbf{b} collects the energy and momentum generation rates:

$$\mathbf{X} = \begin{bmatrix} \Delta T_R \\ \Delta T_N \\ \mathbf{u} \end{bmatrix}, \quad \mathbf{b} = \begin{bmatrix} \sum_{\mu} \rho_{\mu} \chi_{\mu} \dot{Q}_{\mu} \\ \sum_{\mu} \eta_{\mu} \chi_{\mu} \dot{Q}_{\mu} \\ \sum_{\mu} \eta_{\mu} \chi_{\mu} \dot{Q}_{\mu} \mathbf{q} / \omega_{\mu} \end{bmatrix} \quad (18)$$

The unknown response vector can be easily solved by $\mathbf{X} = \mathbf{A}^{-1} \mathbf{b}$ at each transformation coordinate (Ω, ξ) . After obtaining \mathbf{X} , the local temperature response $\mathcal{G}_{\Delta T}$ to the point source can be obtained from the local energy deviation:

$$\mathcal{G}_{\Delta T} = \frac{\sum_{\mu} g_{\mu}}{C} = \frac{1}{\sum_{\mu} C_{\mu}} \sum_{\mu} C_{\mu} \left(\frac{X_R}{\tau_{\mu}^R} + \frac{X_N}{\tau_{\mu}^N} \right) \quad (19)$$

where C is the total specific heat, X_R and X_N denote the first two components of \mathbf{X} which are the Green's functions of the pseudo-temperatures ΔT_R and ΔT_N .

As illustrated in Figure 1, the temperature response is a combined result of the momentum-conserving N processes and the momentum-destroying R processes. After the $\mathcal{G}_{\Delta T}$ is obtained, temperature response to an arbitrary any heating profile $P(t, \mathbf{r})$ can be calculated as the convolution $\Delta T = \mathcal{G}_{\Delta T} * P$ in the real space. In the Fourier transformation domain, the temperature rise is simply the product of the Green's function and the heating profile:

$$\Delta T(\Omega, \xi) = \mathcal{G}_{\Delta T}(\Omega, \xi) P(\Omega, \xi) \quad (20)$$

For pump-probe experiments, the measured signal is typically proportional to the average temperature change weighted by the sensing beam profile $S(\Omega, \xi)$:

$$\Delta \bar{T}(\Omega) = \int \mathcal{G}_{\Delta T}(\Omega, \xi) P(\Omega, \xi) S(\Omega, \xi) d\xi \quad (21)$$

The time-domain temperature change $\Delta\bar{T}(t)$ can be simply obtained by inverse Fourier transform. The advantage of our approach is also manifested in Eq. (21). Once the Green's function $\mathcal{G}_{\Delta T}(\Omega, \xi)$ is calculated, one can obtain temperature responses in any geometry using a simple integration without recalculating the transport dynamics of all phonon modes.

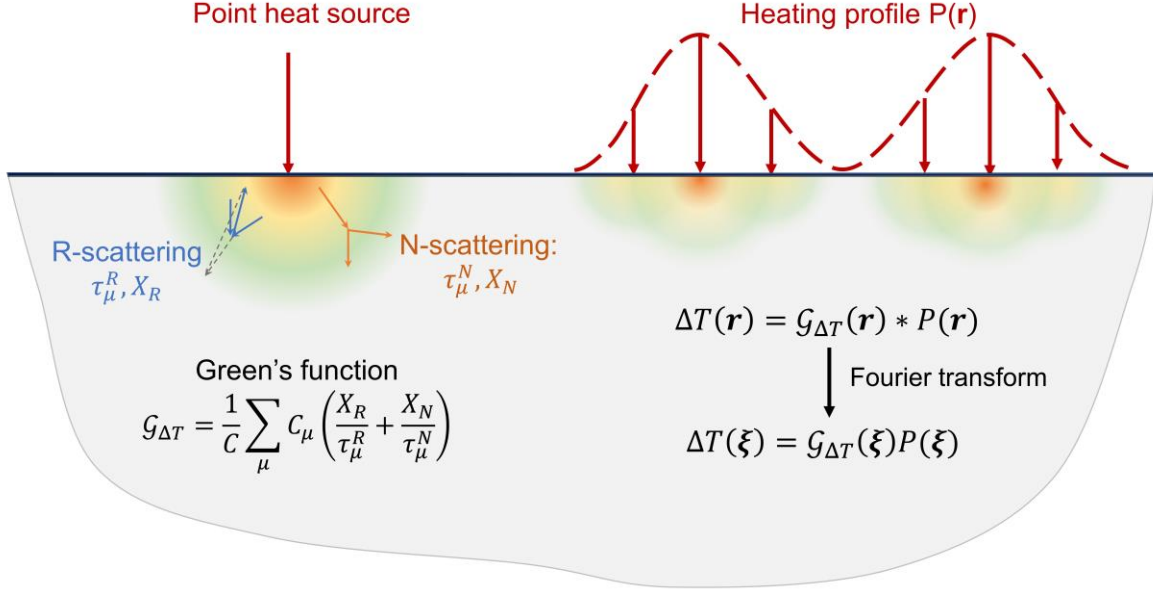


Figure 1. Illustration of the GF-CSA. The Green's function is a combined result of the momentum-conserving N-processes and momentum-destroying R-processes. For any heating profile, the temperature response can be calculated by performing a convolution of Green's function with the heating profile in real space, which corresponds to a simple multiplication in the Fourier transformation domain.

III. ASYMPTOTIC BEHAVIORS OF GF-CSA

We now examine the asymptotic behaviors of the GF-CSA. In Section III.A, we first show the emergence of second sound waves when N-scattering dominates the phonon-phonon interaction by perturbatively expanding the susceptibility χ_μ . In Section III.B, we show the recovery to RTA at the strong R-scattering limit, and the convergence to the diffusive transport when $\Omega\tau_\mu \ll 1$ and the ballistic limit when $\Omega\tau_\mu \gg 1$, respectively.

A. Emergence of Second Sound with Dominating N-scattering

We analytically show that the damped wave equation of the second sound emerges by perturbatively expanding the susceptibility χ_μ at the limit $\tau_\mu^N \ll \tau_\mu^R$, *i.e.* N-scattering dominates the phonon-phonon interaction. For mathematical simplicity, we consider the homogenous condition with the source term $\mathbf{b} = \mathbf{0}$. Without losing the general physics, one-dimensional transport is assumed here to show the asymptotic damped wave behavior of the GF-CSA. When either N or R processes dominate the phonon scattering events, the population or energy deviation can be described by a single local temperature rise $\Delta T_N \approx \Delta T_R = \Delta T$. The dimensionality of the linear equation $\mathbf{A}\mathbf{X} = \mathbf{b}$ is therefore reduced to:

$$\begin{bmatrix} \sum_\mu \frac{C_\mu}{\tau_\mu^N} (1 - \chi_\mu) & \sum_\mu \frac{C_\mu T_0 q_x}{\omega_\mu \tau_\mu^N} (1 - \chi_\mu) \\ \sum_\mu \frac{C_\mu q_x}{\omega_\mu \tau_\mu^N} (1 - \chi_\mu) & \sum_\mu \frac{C_\mu T_0 q_x^2}{\omega_\mu^2 \tau_\mu^N} (1 - \chi_\mu) \end{bmatrix} \begin{bmatrix} \Delta T \\ u \end{bmatrix} = \mathbf{0} \quad (22)$$

In the limit $\Lambda_{\mu,x} \xi_x \ll 1$ and $\Omega \tau_\mu \ll 1$, the susceptibility can be expanded as:

$$1 - \chi_\mu = i\Omega \tau_\mu + i\Lambda_{\mu,x} \xi_x \quad (23)$$

To the linear order, the matrix elements can therefore be expanded as:

$$\sum_\mu \frac{C_\mu}{\tau_\mu^N} (1 - \chi_\mu) \approx i\Omega C \quad (24)$$

$$\sum_\mu \frac{C_\mu T_0 q_x}{\omega_\mu \tau_\mu^N} (1 - \chi_\mu) \approx \sum_\mu \frac{C_\mu T_0 q_x}{\omega_\mu} v_{\mu,x} \cdot i\xi_x \quad (25)$$

$$\sum_\mu \frac{C_\mu q_x}{\omega_\mu \tau_\mu^N} (1 - \chi_\mu) \approx \sum_\mu \frac{C_\mu q_x}{\omega_\mu} v_{\mu,x} \cdot i\xi_x \quad (26)$$

$$\sum_\mu \frac{C_\mu T_0 q_x^2}{\omega_\mu^2 \tau_\mu^N} (1 - \chi_\mu) \approx \sum_\mu \frac{C_\mu T_0 q_x^2}{\omega_\mu^2} \left(\frac{1}{\tau_\mu^R} + i\Omega \right) \quad (27)$$

With inverse Fourier transform, $i\Omega$ and $i\xi_x$ are replaced with differential operators $\frac{\partial}{\partial t}$ and $\frac{\partial}{\partial x}$,

and a set of partial differential equations can be written as:

$$C \frac{\partial T}{\partial t} + \left(\sum_{\mu} \frac{C_{\mu} T_0 q_x v_{\mu,x}}{\omega_{\mu}} \right) \frac{\partial u}{\partial x} = 0 \quad (28)$$

$$\left(\sum_{\mu} \frac{C_{\mu} q_x v_{\mu,x}}{\omega_{\mu}} \right) \frac{\partial T}{\partial x} + \left(\sum_{\mu} \frac{C_{\mu} T_0 q_x^2}{\omega_{\mu}^2} \right) \frac{\partial u}{\partial t} = - \left(\sum_{\mu} \frac{C_{\mu} T_0 q_x^2}{\omega_{\mu}^2 \tau_{\mu}^R} \right) u \quad (29)$$

Combining these two equations, the damped-wave equation for both temperature and the drift velocity u can be derived:

$$\frac{\partial^2 T}{\partial t^2} + \frac{1}{\tau_{ss,x}} \frac{\partial T}{\partial t} - v_{ss,x}^2 \frac{\partial^2 T}{\partial x^2} = 0 \quad (30)$$

$$\frac{\partial^2 u}{\partial t^2} + \frac{1}{\tau_{ss,x}} \frac{\partial u}{\partial t} - v_{ss,x}^2 \frac{\partial^2 u}{\partial x^2} = 0 \quad (31)$$

$\tau_{ss,x}$ and $v_{ss,x}^2$ are relaxation time and second sound velocity along the x -direction:

$$\frac{1}{\tau_{ss,x}} = \frac{\sum_{\mu} C_{\mu} q_x^2 / (\omega_{\mu}^2 \tau_{\mu}^R)}{\sum_{\mu} C_{\mu} q_x^2 / \omega_{\mu}^2}, \quad (32)$$

$$v_{ss,x}^2 = \frac{(\sum_{\mu} C_{\mu} q_x v_{\mu,x} / \omega_{\mu})^2}{C \sum_{\mu} C_{\mu} q_x^2 / \omega_{\mu}^2}. \quad (33)$$

Eq. (30-32) shows that both the temperature field and the drift velocity behave as attenuating waves, and the damping rate is determined by the R-scattering strength $1/\tau_{\mu}^R$. Results obtained by perturbative expansion of GF-CSA are consistent with previous derivations by Hardy²³ and Ding et al¹⁷.

B. Convergence to RTA, Diffusive, and Ballistic Limits

The GF-CSA developed in this work reduces the RTA when R-scattering dominates over N-scatterings, and further recovers the Fourier solution at the diffusive limit and the ballistic solution with $\Omega \tau_{\mu} \gg 1$. With dominating R-scattering, $\tau_{\mu} \approx \tau_{\mu}^R \ll \tau_{\mu}^N$, only the matrix element A_{11} approaches to $\sum_{\mu} C_{\mu} \tau_{\mu}^{-1} (1 - \chi_{\mu})$, and the other matrix elements vanishes. The source term $\mathbf{b} \rightarrow [\sum_{\mu} \chi_{\mu} \dot{Q}_{\mu}, 0, \mathbf{0}]^T$. As a result, Green's function of temperature change at the R-scattering limit (i.e. the RTA) is simply solved as b_1/A_{11} :

$$\mathcal{G}_{\Delta T}^{RTA}(\Omega, \xi) = \frac{\sum_{\mu} \chi_{\mu} \dot{Q}_{\mu}}{\sum_{\mu} \frac{C_{\mu}}{\tau_{\mu}} (1 - \chi_{\mu})} \quad (34)$$

This is identical to the analytical results derived by Hua et al ²⁸. At the limit $\Omega\tau_{\mu} \ll 1$ and

$|\mathbf{\Lambda}_{\mu} \cdot \xi| \ll 1$, leading order expansion of the susceptibility is $\chi_{\mu} \approx 1 + i\Omega\tau_{\mu} + (\mathbf{F}_{\mu} \cdot \xi)^2$:

$$\Delta T \approx \frac{Q_0}{\sum_{\mu} \frac{C_{\mu}}{\tau_{\mu}} [i\Omega\tau_{\mu} + (\mathbf{F}_{\mu} \cdot \xi)^2]} = \frac{Q_0}{i\Omega C + \sum_j K_j \xi_j^2} = \Delta T_F \quad (35)$$

where $K_j = \sum_{\mu} C_{\mu} F_{\mu,j}^2 / \tau_{\mu} = \sum_{\mu} C_{\mu} v_{\mu,j} F_{\mu,j}$ is the thermal conductivity along the j -th direction,

and ΔT_F denotes the frequency-domain solution of the heat conduction equation using Fourier's law.

Finally, the ballistic regime occurs when $\Omega\tau_{\mu} \gg 1$, and the BTE is reduced to:

$$\left(\frac{\partial}{\partial t} + \mathbf{v}_{\mu} \cdot \nabla \right) g_{\mu} = \dot{Q}_{\mu} \delta(\mathbf{r}) \delta(t) \quad (36)$$

The modal energy deviations can be solved by performing Fourier transforms to Eq. (3), and ballistic temperature profile ²⁸ is recovered:

$$\mathcal{G}_{\Delta T}^b(\xi, \Omega) = \frac{\dot{Q}_0}{C} \sum_{\mu} \frac{p_{\mu}}{i[\Omega + \mathbf{v}_{\mu} \cdot \xi]} \quad (37)$$

where $p_{\mu} = \dot{Q}_{\mu} / \dot{Q}_0 = C_{\mu} / C$.

IV. MODELING TRANSIENT RESPONSE IN PUMP-PROBE MEASUREMENTS

In this section, we apply the GF-CSA formalism for modeling the ultrafast thermal response under pulsed heating in pump-probe measurements. Ultrafast temperature oscillations are analyzed in the in-plane direction of graphite, in transient thermal grating (TTG) and transient thermorefectance (TTR). In the former case, the thermal transport takes place across the periodic grating, and the second sound corresponds to one-dimensional plane waves. In TTR, the thermal transport has radial symmetry if the probe beam and the pump beam are co-axial, and the second sound corresponds to cylindrical waves. Such radial symmetry can be broken once the probe beam has a finite offset. The GF-CSA formalism can be conveniently

incorporated to model the ultrafast temperature oscillations, and successfully captures the signature of the second sound in the aforementioned geometries, manifested as the temperature dipping below the initial temperature at a few nanoseconds. To obtain the phonon properties of graphite, we performed first-principles calculations using the Quantum Espresso package³⁶. Harmonic force constants are calculated using the density functional perturbation theory (DFPT) using the Perdew-Zunger (PZ) exchange-correlation functionals³⁷ with a cutoff energy of 80 Rydberg and a $10 \times 10 \times 4$ supercell. The third-order force constants are calculated using the finite displacement method with a $5 \times 5 \times 4$ supercell within a cutoff of 4 Å, using the `thirdorder.py` script of ShengBTE package²⁴ with a $32 \times 32 \times 10$ mesh in the momentum space. Phonon lifetimes, and mean free displacements are obtained by iteratively solving the BTE using the ShengBTE package²⁴.

One-dimensional periodic heating in TTG. We first model the simplest one-dimensional hydrodynamic phonon transport in transient thermal grating. As illustrated in Figure 2a, TTG uses two laser beams cross-focused at the sample surface to create an interference pattern, and the heat source imposed on the sample has a spatially periodic profile, as shown in Figure 2b. Such spatially periodic heating profile corresponds to two spikes in the Fourier transformation domain at $\xi_x = \pm 2\pi/L$, and the temperature oscillation in the time-domain can be further calculated using the inverse Fourier transform:

$$\Delta T(t) = \frac{1}{4\pi} \int_{-\infty}^{\infty} \left[\mathcal{G}_{\Delta T} \left(\Omega, \frac{2\pi}{L} \right) + \mathcal{G}_{\Delta T} \left(\Omega, -\frac{2\pi}{L} \right) \right] e^{i\Omega t} d\Omega \quad (38)$$

Figure 2c shows the evolution of temperature rise from 50 K to 300 K, with the grating size $L = 3 \mu\text{m}$. Near room temperatures (250 K to 200 K), ΔT shows a monotonic decay with increasing time, indicating a diffusive behavior. Between 80 K and 150 K, ΔT shows oscillations with a negative below zero. Such negative dip is attributed to a phase shift by π : temperatures in the region heated by the thermal grating becomes even cooler than the initial

temperature. Such negative dips indicates the temperature field behaves like a standing wave, which is the signature of the hydrodynamic second sound. At a very low temperature of 50 K, the phonon transport is primarily ballistic hence no lattice cooling effect is observed¹⁶. By scanning over different temperatures and grating periods, the hydrodynamic window can be mapped as shown in [Figure 2d](#). The second sound is observed when the characteristic size L of the temperature field is small enough such that phonons are dissipated before experiencing momentum-destroying R-scattering events, but still large enough to allow enough N-scattering. Namely, hydrodynamic lattice cooling due to second sound only existed when $1/\tau_\mu^R < v_\mu/L < 1/\tau_\mu^N$. In [Figure 2e-f](#), we compared the temperature evolution predicted by GF-CSA with the TTG experimental data, showing reasonable agreements in both the dipping time and the dipping depths. Based on the dipping time, the apparent second sound speed is calculated as $v_{ss} = L/(2t_{dip}) = 3.9$ km/s at 100 K and 3.5 km/s at 150 K, agreeing well with previous reports^{16, 17}. The decreased v_{ss} with increasing temperatures is also consistent with experimental observation¹⁷, due to the larger fraction of diffusive phonons caused by frequent phonon-phonon scattering at increased temperatures.

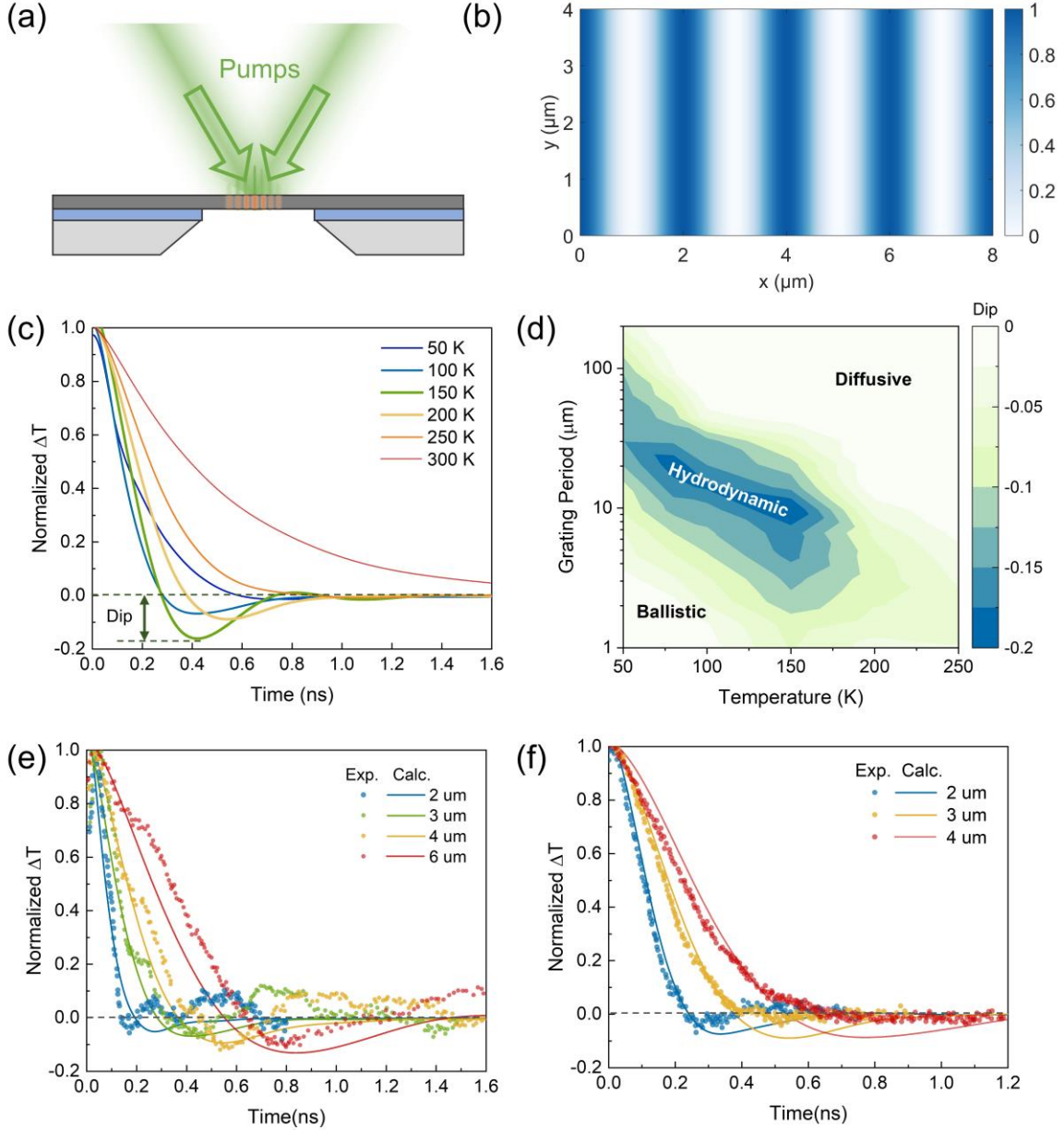


Figure 2. Temperature response in graphite under transient thermal grating (TTG). (a) Illustration of the TTG heating scheme. (b) Periodic heating intensity with the color bar showing the minimum heating rate to the maximum heating. (c) Temperature-dependent thermal responses at the grating period $L = 3 \mu\text{m}$. (d) The predicted hydrodynamic window using GF-CSA. (e-f) Grating period dependent temperature responses at (e) 100 K, and (f) 200 K. The temperature dip below zero indicates the lattice cooling due to the hydrodynamic second sound waves. Experimental data is from ref. 17.

Radially symmetric Ring-TTR. In addition to the simple TTG, we have further modeled the transient thermoreflectance using a ring-shaped pump beam (Ring-TTR), as shown in [Figure 3a](#). Different from using a normal Gaussian pump beam, a ring-shaped pump excites thermal phonons at the ring and allows the phonons to propagate a certain distance to the ring center. Due to the radial symmetry, the thermal waves reaching the center are in-phase, and will constructively interfere to

amplify the temperature oscillations due to phonon hydrodynamics. The Fourier-transformed beam profiles are written as:

$$P(\xi) = A_p \exp\left[-\frac{w_p^2 \xi^2}{8}\right] \cdot J_0(|\xi|R_0), \quad (39)$$

$$S(\xi) = A_s \exp\left[-\frac{w_s^2 \xi^2}{8}\right] \quad (40)$$

where A_p and A_s are the intensities of the pump and the probe beams respectively; R_0 is the radius of the pump ring; w_p is the $1/e^2$ half-width of the ring, w_s is the $1/e^2$ radius of the probe; \mathbf{r}_{off} is the offset vector of the probe from the ring center; $\xi = (\xi_x, \xi_y)$ is the two-dimensional Fourier transform vector, and J_0 is the 0-th order Bessel function. The probe-averaged temperature response can then be calculated using Eq. (21) in the frequency domain, and the time-domain results are further obtained using the inverse Fourier transform. With co-axial pump and probe beams (Figure 3b), the predicted temperature responses from 80 K to 200 K are shown in Figure 3c. Our model captured the transient lattice cooling at 80 K and 100 K, with a dip located at 6 ns agreeing well with experiments. Nevertheless, the predicted dip depth is shallower than experimental observations. Possible reasons include (1) the limited signal-to-noise ratio in the ring-TTR experiment, with the measured signal even fluctuating below zeros at high temperatures (200 – 300 K) in the experimental data³⁸; (2) the limited mesh in the Brillouin zone imposes a cutoff for the phonon wavelengths, such that long-wave-length phonons whose scattering is dominated by N processes are not included in the modeling. The predicted weak second sound dips are consistent with Monte Carlo BTE simulations³⁸. Such long-wavelength cutoff might also be responsible for the absence of second sound dips at 150 K in first-principles modeling, while the practical ring-TTR measurement still shows a dip touching the zero-temperature rise limit. Second sound velocity can also be extracted as $v_{ss} = R_0/\Delta t_{pd}$ using to the peak-to-dip time Δt_{pd} . Using the calculated ring-TTR signal, the apparent second sound speed is calculated as ≈ 3.8 km/s at 100 K, agreeing well with the intrinsic second sound ~ 3.9 km/s¹⁷.

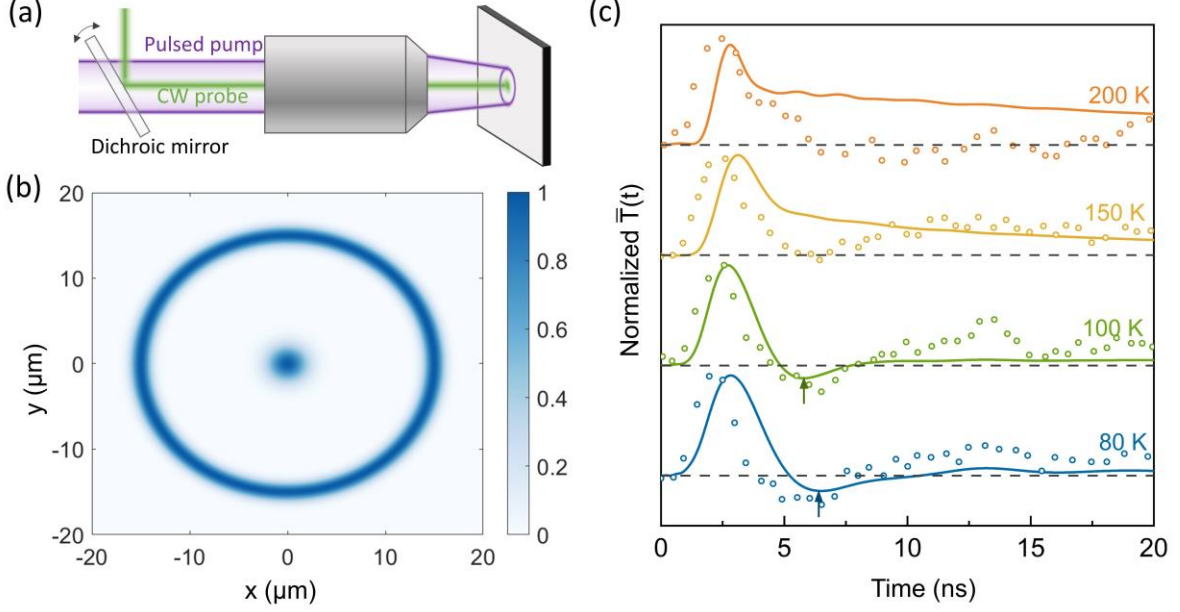


Figure 3. Temperature response in ring-pumped transient thermoreflectance (ring-TTR). (a) Illustration of ring-TTR. The sample is heated by a pulsed laser with a ring shape, and the CW probe beam probes the temperature in the ring center. (b) Beam intensities of co-axial ring pump and Gaussian probe, with a pump-ring radius of 15 μm and a width of 3 μm , and a probe beam diameter of 6 μm . (c) Modeled temperature responses compared with experimental data ³⁸.

Off-centered probe in ring-TTR. After modeling co-axial pump and probe beams with radial symmetry, we further investigated ring-TTR with an off-centered probe breaking the radial symmetry. The TTR signal can be easily calculated by integrating the GF-CSA over the pump and probe profiles in the Fourier domain, with the off-centered probe written as $S(\xi, \mathbf{r}_{off}) = S(\xi) \cdot \exp[-i\xi \cdot \mathbf{r}_{off}]$. The laser intensities and the predicted TTR signals are shown in Figure 4a-b. As the probe beam moves away from the center towards the pump ring, there is increased overlap between the pump intensity and the probe intensity, and the instantaneous temperature rise is picked up by the probe beam, which results in the increased signal magnitude at $t = 0$. The peak time is also delayed with increasing offset, because it takes a longer time for the thermal excitation from the other side of the ring to reach the probe spot. The probe beam offset imposes a spatial phase on the thermal response, therefore shifting the location of temperature peaks and dips. By scanning the probe within the ring-pumped area, we can also obtain the probe-weighted temperature profile at $t = 2.85$ ns and $t = 6.78$ ns, which corresponds to the maximum temperature rise and lattice cooling with zero probe offset, as shown in Fig. 4c-d. Maximum hydrodynamic lattice cooling is measured when the probe beam is located at the center. With cylindrical heating, the ring center is equivalent to an adiabatic boundary condition, and the heat wave

incident to the ring center is reflected with a phase inversion, which leads to maximum lattice cooling near the center.

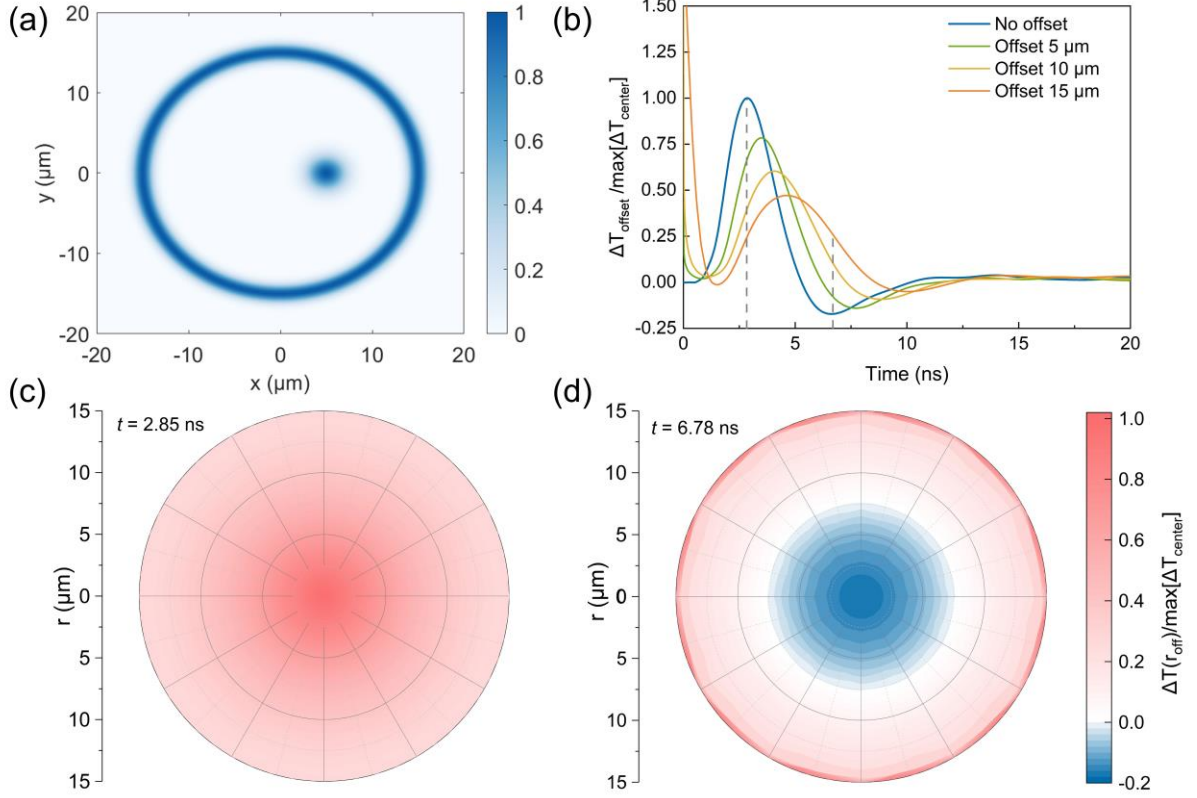


Figure 4. Off-centered probe measurement. (a) Off-centered pump and probe beam intensities. (b) Temperature oscillations at different beam offsets. The response is normalized by the maximum temperature rise with the probe beam at the ring center. Temperature profiles at (c) 2.85 ns and (d) 6.78 ns, with the time slices indicated by dashed lines in (b).

V. SUMMARY

We have derived Green's function of the multidimensional Boltzmann transport equation under Callaway scattering approximation for modeling hydrodynamic second sound. We also showed the emergence of second sound waves by the perturbative expansion of Green's function, and we mathematically proved the convergence to ballistic and diffusive transport at the limits of $\Omega\tau_\mu \gg 1$ and $\Omega\tau_\mu \ll 1$, respectively. This formalism can be conveniently implemented to predict transient temperature responses to arbitrary-shaped heat sources in infinite or semi-infinite domains, using fully first-principle phonon dispersions and lifetimes. The modeling

prediction shows nice agreement in temperature oscillation dynamics and second sound velocities with the literature reports in TTG and ring-TTR measurements. Our work provides a simple formalism for modeling transient hydrodynamic phonon transport in different heating geometries.

Acknowledgment

This work is supported by the National Key R&D Program (No. 2022YFA1203100) and the National Natural Science Foundation (No. 52076089 and No.12147122). The authors declare no conflict of interest.

References

1. G. Chen, *Nanoscale Energy Transport and Conversion*. (Oxford University Press, ISBN: 9780195159424, 2005).
2. X. Qian, J. Zhou and G. Chen, *Nat. Mater.* **20**, 1188-1202 (2021).
3. G. Chen, *Nature Reviews Physics* **3** (8), 555-569 (2021).
4. L. Zeng, K. C. Collins, Y. Hu, M. N. Luckyanova, A. A. Maznev, S. Huberman, V. Chiloyan, J. Zhou, X. Huang, K. A. Nelson and G. Chen, *Scientific reports* **5**, 17131 (2015).
5. M. E. Siemens, Q. Li, R. Yang, K. A. Nelson, E. H. Anderson, M. M. Murnane and H. C. Kapteyn, *Nat Mater* **9** (1), 26-30 (2010).
6. T. K. Hsiao, H. K. Chang, S. C. Liou, M. W. Chu, S. C. Lee and C. W. Chang, *Nature nanotechnology* **8** (7), 534-538 (2013).
7. G. Chen, *Phys. Rev. Lett.* **86** (11), 2297-2300 (2001).
8. R. Yang, G. Chen and M. S. Dresselhaus, *Phys. Rev. B* **72**, 125418 (2005).
9. R. Yang and G. Chen, *Phys. Rev. B* **69** (19), 195316 (2004).
10. R. A. Guyer and J. A. Krumhansl, *Phys. Rev.* **148** (2), 778-788 (1966).
11. J. Callaway, *Phys. Rev.* **113** (4), 1046-1051 (1959).
12. D. D. Joseph and L. Preziosi, *Rev. Mod. Phys.* **61** (1), 41-73 (1989).
13. V. Peshkov, *J. Phys. (Moscow)* **8**, 381-389 (1944).
14. V. Narayanamurti and R. C. Dynes, *Phys. Rev. Lett.* **28** (22), 1461-1465 (1972).
15. H. E. Jackson, C. T. Walker and T. F. McNelly, *Phys. Rev. Lett.* **25** (1), 26-28 (1970).
16. S. Huberman, R. A. Duncan, K. Chen, B. Song, V. Chiloyan, Z. Ding, A. A. Maznev, G. Chen and K. A. Nelson, *Science* **364** (6438), 375-379 (2019).
17. Z. Ding, K. Chen, B. Song, J. Shin, A. A. Maznev, K. A. Nelson and G. Chen, *Nature communications* **13**, 285 (2022).
18. S. Lee, D. Broido, K. Esfarjani and G. Chen, *Nature communications* **6**, 6290 (2015).
19. A. Beardo, M. López-Suárez, L. A. Pérez, L. Sendra, M. I. Alonso, C. Melis, J. Bafaluy, J. Camacho, L. Colombo, R. Rurali, F. X. Alvarez and J. S. Reparaz, *Science Advances* **7**, eabg4677 (2021).
20. R. Kovács and P. Ván, *Int. J. Heat Mass Transfer* **83**, 613-620 (2015).
21. F. X. Alvarez, D. Jou and A. Sellitto, *J. Appl. Phys.* **105**, 014317 (2009).
22. C. P. Enz, *Annals of Physics* **46**, 114-173 (1968).
23. R. J. Hardy, *Phys. Rev. B* **2** (4), 1193-1207 (1970).

24. W. Li, J. Carrete, N. A. Katcho and N. Mingo, *Comput. Phys. Commun.* **185** (6), 1747-1758 (2014).
25. A. J. H. McGaughey, A. Jain and H.-Y. Kim, *J. Appl. Phys.* **125** (1), 011101 (2019).
26. J. Xu, Y. Hu and H. Bao, *Physical Review Applied* **19** (1), 014007 (2023).
27. P. B. Allen and V. Perebeinos, *Phys. Rev. B* **98**, 085427 (2018).
28. C. Hua and A. J. Minnich, *Phys. Rev. B* **90** (21), 214306 (2014).
29. V. Chiloyan, S. Huberman, Z. Ding, J. Mendoza, A. A. Maznev, K. A. Nelson and G. Chen, *Phys. Rev. B* **104**, 245424 (2021).
30. Z. Ding, J. Zhou, B. Song, V. Chiloyan, M. Li, T. H. Liu and G. Chen, *Nano Lett* **18** (1), 638-649 (2018).
31. C. Zhang, S. Chen and Z. Guo, *Int. J. Heat Mass Transfer* **176**, 121282 (2021).
32. Y. Guo and M. Wang, *Phys. Rev. B* **97**, 035421 (2018).
33. C. Zhang, S. Huberman and L. Wu, *J. Appl. Phys.* **132** (8), 085103 (2022).
34. X.-P. Luo, Y.-Y. Guo, M.-R. Wang and H.-L. Yi, *Phys. Rev. B* **100**, 155401 (2019).
35. Y. Guo, Z. Zhang, M. Bescond, S. Xiong, M. Wang, M. Nomura and S. Volz, *Phys. Rev. B* **104** (7), 075450 (2021).
36. P. Giannozzi, S. Baroni, N. Bonini, M. Calandra, R. Car, C. Cavazzoni, D. Ceresoli, G. L. Chiarotti, M. Cococcioni, I. Dabo, A. Dal Corso, S. de Gironcoli, S. Fabris, G. Fratesi, R. Gebauer, U. Gerstmann, C. Gougoussis, A. Kokalj, M. Lazzeri, L. Martin-Samos, N. Marzari, F. Mauri, R. Mazzarello, S. Paolini, A. Pasquarello, L. Paulatto, C. Sbraccia, S. Scandolo, G. Sclauzero, A. P. Seitsonen, A. Smogunov, P. Umari and R. M. Wentzcovitch, *J. Phys.: Condens. Matter* **21** (39), 395502 (2009).
37. J. P. Perdew and A. Zunger, *Phys. Rev. B* **23** (10), 5048-5079 (1981).
38. J. Jeong, X. Li, S. Lee, L. Shi and Y. Wang, *Phys. Rev. Lett.* **127**, 085901 (2021).